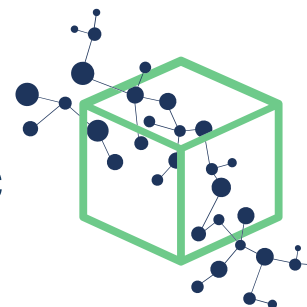


reprint

# Molecular interaction mechanism in the separation of a binary azeotropic system by extractive distillation with ionic liquid



Li, Sun, Li, Xi, Zhou, Li, Zhang, and Gao (2021)

DOI: [10.1016/j.gee.2020.11.025](https://doi.org/10.1016/j.gee.2020.11.025)

**XI RESEARCH**  
<https://xiresearch.org>

This document is the **final published** version of an article published in its final form (i.e., the version of record) by KeAi as

Hong Li, Guanlun Sun, Dongyang Li, Li Xi, Peng Zhou, Xingang Li, Ji Zhang, and Xin Gao. Molecular interaction mechanism in the separation of a binary azeotropic system by extractive distillation with ionic liquid. *Green Energy and Environment*, 6:329–338, 2021. doi: 10.1016/j.gee.2020.11.025

(copyright © 2021, Li, Sun, Li, Xi, Zhou, Li, Zhang, and Gao). The *version of record* is hosted at

<https://dx.doi.org/10.1016/j.gee.2020.11.025>

by the publisher.

The current version is made available under the CC-BY-NC-ND 4.0 license (<https://creativecommons.org/licenses/by-nc-nd/4.0/>) in accordance with the publisher's policy. Please refer to the publisher's site for additional terms of use.

## BIB<sub>T</sub><sub>E</sub>X Citation Entry

```
@article{LiGreenEnergyEnviron21,  
  author = {Li, Hong and Sun, Guanlun and  
            Li, Dongyang and Xi, Li and Zhou,  
            Peng and Li, Xingang and Zhang, Ji  
            and Gao, Xin},  
  title = {{Molecular interaction  
            mechanism in the separation of  
            a binary azeotropic system by  
            extractive distillation with ionic  
            liquid}},  
  journal= {Green Energy and Environment},  
  volume = {6},  
  pages = {329–338},  
  year = {2021},  
}
```

brought to you by the  
**XI RESEARCH GROUP** at McMaster University

— [www.XIRESEARCH.org](http://www.XIRESEARCH.org) —

Principle Investigator:

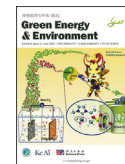
Li Xi 奚力

Email: [li@xiresearch.org](mailto:li@xiresearch.org)

**t** <https://twitter.com/xiresearchgroup>

**in** <https://linkedin.com/company/xiresearch/>

**RG** [https://researchgate.net/profile/Li\\_Xi16](https://researchgate.net/profile/Li_Xi16)



Research paper

# Molecular interaction mechanism in the separation of a binary azeotropic system by extractive distillation with ionic liquid

Hong Li <sup>a</sup>, Guanlun Sun <sup>a</sup>, Dongyang Li <sup>a,b</sup>, Li Xi <sup>b,\*</sup>, Peng Zhou <sup>a</sup>, Xingang Li <sup>a</sup>, Ji Zhang <sup>a</sup>,  
Xin Gao <sup>a,\*</sup>

<sup>a</sup> School of Chemical Engineering and Technology, National Engineering Research Center of Distillation Technology, Collaborative Innovation Center of Chemical Science and Engineering (Tianjin), Tianjin University, Tianjin, 300072, China

<sup>b</sup> Department of Chemical Engineering, McMaster University, Hamilton, Ontario, L8S 4L7, Canada

Received 5 September 2020; revised 26 November 2020; accepted 26 November 2020

Available online 28 November 2020

## Abstract

Ionic liquids (ILs) have shown excellent performance in the separation of binary azeotropes through extractive distillation [1]. But the role of the ionic liquid in azeotropic system is not well understood. In this paper, COSMO-RS model was applied to screen an appropriate IL to separate the binary azeotrope of ethyl acetate (EA) and ethanol and 1-octyl-3-methylimidazolium tetrafluoroborate ([OMIM][BF<sub>4</sub>]) was selected. The Quantum Mechanics (QM) calculations and molecular dynamics (MD) simulation are performed to study the interactions between the solvent molecules and [OMIM][BF<sub>4</sub>], in order to investigate the separation mechanism at the molecular level. The nature of the interactions is studied through the reduced density gradient (RDG) function and quantum theory of Atom in Molecule (QTAIM). Hydrogen bonds and van der Waals interactions are the key interactions in the complexes. The results of MD simulations indicate that the introduction of ILs has a prominent effect on the interaction between the solvent molecules, especially on reducing the number of hydrogen bonds among the solvent molecules. The radial distribution function (RDF) reveals that the interaction between the cation and solvent molecules will increase while the concentration of ILs increases. This paper provides important information for understanding the role of ILs in the separation of the azeotropic system, which is valuable to the development of new entrainers.

© 2020, Institute of Process Engineering, Chinese Academy of Sciences. Publishing services by Elsevier B.V. on behalf of KeAi Communications Co., Ltd. This is an open access article under the CC BY-NC-ND license (<http://creativecommons.org/licenses/by-nc-nd/4.0/>).

**Keywords:** Ionic liquids; Azeotrope; Density functional theory; Separation; Extractive distillation

## 1. Introduction

The separation of alcohol-ester binary azeotropes by extractive distillation is an important industrial separation process, and the selection of the extractant is a key step [1,2]. Ionic liquids (ILs) are widely used as such extractants which have better separation performance than other materials owing to their strong interactions with the solvents. Furthermore, ILs can be easily recycled due to their outstanding properties, e.g.,

thermal stability, negligible vapor pressure, and tunable solubility [3–6]. It is commonly believed that ILs interact more strongly with one solvent in a mixture such that the relative volatility of the other component is enhanced to directly break the azeotrope [7–9]. Therefore, ILs are extensively used as entrainers in extractive distillation processes [10–12].

Macroscopic behaviors of these mixtures are determined by the microstructures and nature of the interactions between ILs and other compounds [13–15]. Molecular dynamics (MD) simulation provides direct access to the microscopic structures of the target molecules which are not easily obtained in the experiment [16]. Xu et al. [17] studied the structure and thermodynamic properties of the interface between [BMIM]

\* Corresponding authors.

E-mail addresses: [xili@mcmaster.ca](mailto:xili@mcmaster.ca) (L. Xi), [gaoxin@tju.edu.cn](mailto:gaoxin@tju.edu.cn) (X. Gao).

[OAc] and a gas mixture of  $C_2H_4$  and  $C_2H_2$  by MD simulation. Based on the calculated interaction energies, they found the interaction of  $C_2H_2$  with the cation, anion and ion pair was stronger than those of  $C_2H_4$  and these stronger interactions become the reason of selective separation of  $C_2H_2$  from the mixture. Zhang and coworkers [18] studied the extraction mechanism of three typical ILs [BMIM][HSO<sub>4</sub>], [MIM][HSO<sub>4</sub>], [BMIM][OTF] in the separation of the methanol and n-hexane. The result showed that the cation with the longer alkyl chain has larger interaction energy with the methanol, which lead to the different ability of separation. Xu et al. [15] studied the mechanism analysis for separation of cyclohexane and *tert*-butanol by three ionic liquids ([BMIM][NTF<sub>2</sub>], [BMIM][OTF] and [BMIM][HSO<sub>4</sub>]). In this work, the hydrogen bond in the system was analyzed. It is observed that strong hydrogen bonds were formed between the [BMIM][NTF<sub>2</sub>]/[BMIM][OTF] and *tert*-butanol, compared to the weak interaction formed by [BMIM][HSO<sub>4</sub>] and *tert*-butanol. Earlier this year, Chen et al. [19] carried out MD simulations to elucidate the mechanism in the separation of acetone-methanol mixture by ILs [MMIM][DMP]. They found that the excess enthalpies decrease significantly upon the addition of the ILs, and various types of molecular clusters with different connection modes were also investigated, making a further step to illustrate the role of ILs on the separation of ketone-alcohol azeotropic system. Despite those progresses, the vast diversity of practical azeotropic systems leaves much area to explore.

In a previous work, Li et al. [20] explored the separation performance of ethanol-ethyl acetate (EA) mixture among three kinds of ionic liquids with different cations and the experimental results showed that [OMIM][BF<sub>4</sub>] has a better separation capability at a mole fraction range from 0.10 to 0.30. Especially when the concentration of IL increases and reaches about 0.2, the azeotropic point is eliminated. The effect of the amount of ionic liquids seems to be very important. Although the present work attempts to provide detailed molecular insight into the mechanism of the enhanced relative volatility of ethanol and EA by ILs, microscopic mechanism of this concentration effect in this system still needs further exploration.

In this work, the selectivity of ethanol to ethyl acetate in different imidazolium ILs and solvent capacity for both solvents were calculated at first based on the COSMO-RS theory. A density functional theory (DFT) quantum chemistry calculation method and Molecular dynamics (MD) method were employed to investigate the role of [OMIM][BF<sub>4</sub>] in the ethanol-EA azeotropic system. In addition, the interactions between the IL and the two types of molecules ( $C_2H_5OH$  and  $CH_3COOCH_2CH_3$ ) are examined with their geometric configurations and interaction energies calculated. The reduced density gradient (RDG) function and quantum theory of atoms in molecules (QTAIM) approaches were applied to study the nature of the interactions and provide a visualization of the weak interaction area of [OMIM][BF<sub>4</sub>]-ethanol (EA) complexes. We also performed MD simulation of the mixture of

ethanol-EA over the IL concentration from 0.1 to 0.3. The behavior of [OMIM][BF<sub>4</sub>] in the simulation box was analyzed with RDF and H-bond (HB) analysis.

## 2. Computational methodology

### 2.1. COSMO-RS model

COSMO-RS model is a method of predicting the thermo-physical data of fluid and liquid mixtures based on quantum chemical method [21,22]. For recent years it has been developed as a promising method for screening optimal candidates from a number of solvents or solutes [23–25]. The selectivity of ethanol (1) to ethylacetate (2) is calculated by the infinite dilution activity coefficient of both solvents in different ionic liquids predicted by the COSMOtherm calculations [26]. The selectivity  $S_{12}$  is defined as [20].

$$S_{12} = \frac{\gamma_1^\infty}{\gamma_2^\infty} \quad (1)$$

in which  $\gamma_i^\infty$  is the infinite dilution activity coefficient of solvents. The solvent capacity of ethanol in ILs is defined as

$$SP = \frac{1}{\gamma_1^\infty} \quad (2)$$

### 2.2. Quantum mechanics calculation

The DFT calculations of the IL [OMIM][BF<sub>4</sub>] and its complexes with solvent molecules,  $C_2H_5OH$  and  $CH_3COOCH_2CH_3$  were carried out using the M06–2X [27] functional with the standard 6-311+G (d, p) basis set, as implemented in the Gaussian 09 software package [28].

All geometric configurations were optimized without any symmetry constraints. The harmonic vibrational frequency calculations were performed at the same theoretical level to confirm the stationary structure for all configurations and to obtain the zero-point vibrational energies (ZPEs).

The interaction energy,  $E_{int}$  of complex AB was calculated from the following equation:

$$E_{int} = E_{AB} - (E_A + E_B) \quad (3)$$

The binding energies were corrected for the ZPE and basis set superposition error (BSSE) by the counterpoise method [29].

$$E_{int}^B = E_{int} + E_{BSSE} \quad (4)$$

To better understand the nature of the interactions of the complexes mentioned above, the RDG [30] function and QTAIM [31] analysis were carried out with the Multiwfn 3.7 program [32] and VMD [33] software package for the relevant configurations to illustrate the bonding characteristics and distinguish the hydrogen bonding interactions from other weak interactions.

### 2.3. Molecular dynamics simulation

Molecular Dynamics simulations were performed by GROMACS 2019.3 simulation package [34,35] with the OPLS-AA [36] force field. OPLS-AA force field has been broadly applied in the simulation of both organic small molecules [37,38] and could also well predict the physical properties of the ILs [39–41]. The Lennard-Jones OPLS-AA parameters of ethanol and EA molecules were obtained from the LigParGen server [42,43], and the partial charges of each atom were scaled to 1.14\*CM1A charge [44]. The parameters of [OMIM]<sup>+</sup> [BF<sub>4</sub>]<sup>-</sup> were obtained from the literature with charge values scaled by a factor of 0.8, which has been proved to reproduce local ion–ion intermolecular interactions of the ionic liquids [45,46]. The Packmol [47] software was used to load the corresponding molecules into the simulation box randomly.

The size of the simulation box was set to be 5 nm in all of the three orthogonal directions. During the simulation, we fixed the number of ethanol and EA at 45:55 M ratio, which is also corresponding to the azeotropic composition at an ambient pressure. In the tertiary system of ethanol(1)-EA (2)-[OMIM][BF<sub>4</sub>](3), the molar fraction of [OMIM][BF<sub>4</sub>] was defined as

$$x_3 = \frac{n_3}{n_1 + n_2 + n_3} \quad (5)$$

For all system, the total numbers of the ethanol and EA molecules were fixed at 434 and 530. For the pseudo-binary system, the mole fraction of ion pairs varying from 0.10 to 0.30. The temperature was maintained at 298 K. And the final pressure in simulation box was maintained at 100 kPa.

The periodic boundary condition was applied in all three dimensions. The system was first energetically minimized by using the steepest-descent method. Then the minimized system was equilibrated using NVT ensemble for 1 ns with a gradual temperature ramp from 0 K to the 298 K. After that the NPT process with ambient pressure and 298 K was applied. Finally, a 10 ns MD simulation was performed in a NVT ensemble at a temporal step of 1 fs with no other constraints. During the whole simulation, the velocity-rescale method [48] was used to maintain the equilibrium temperature, and Berendsen barostat was applied to control the pressure of the box. The particle mesh-Ewald method [49] was used to calculate the long-range electrostatics with a cutoff of 1.0 nm. The cutoff for van der Waals interactions was also set at 1.0 nm.

## 3. Results and discussions

### 3.1. Selectivity and solvent capacity calculation

To screen an appropriate imidazolium ionic liquid, the selectivity of ethanol to ethyl acetate in 28 different kinds of ILs (blue column) and solvent capacity for ethanol (red column) are calculated and shown in Fig. 1. The chosen 28 ILs are composed by characteristic imidazolium cation and traditional anions such as [BF<sub>4</sub>]<sup>-</sup>, I<sup>-</sup> [NO<sub>3</sub>]<sup>-</sup> and so on. Some

of these imidazolium ILs have been proved that could change the phase equilibrium of azeotropic system [20,50–52]. For an entrainer in the extraction system, the selectivity and solvent capacity could offer a quick estimation of its separation ability. It could be depicted in Fig. 1 that these two factors often exhibit opposite trends, and a good entrainer should have a balanced performance [12]. We can also notice that the ILs contain [OMIM]<sup>+</sup> exhibit better selectivity in ethanol when the anion is fixed. This result is agreed with the conclusion of the Li and coworker's work [20]. From the primary results of COSMOtherm calculation, the [OMIM][BF<sub>4</sub>] has been clarified as a good extractant as its both factors, selectivity of ethanol to ethylacetate and the solvent capacity of ethanol in ILs are both high. This means [OMIM][BF<sub>4</sub>] has more outstanding separation ability than other imidazolium ILs. We select [OMIM][BF<sub>4</sub>] for further exploration in this work.

### 3.2. Optimized geometry of [OMIM][BF<sub>4</sub>] ion pairs

The optimized geometries of the isolated [OMIM]<sup>+</sup> cation and [BF<sub>4</sub>]<sup>-</sup> anion, and an ion pair [OMIM]<sup>+</sup>[BF<sub>4</sub>]<sup>-</sup>, from quantum mechanics (QM) calculations, are displayed in Fig. 2. No imaginary frequencies were generated in the frequency calculation. The stable geometric structures of [BF<sub>4</sub>]<sup>-</sup> and [OMIM]<sup>+</sup> were optimized separately which shown in Fig. 2a–b. To guide the design of the initial geometries of the ion pair and the binary complexes, the electrostatic potential surfaces of the cation and anion were mapped and shown in Fig. 2d–e. For the [OMIM]<sup>+</sup> cation, the most positive region is mainly located around the C<sub>6</sub>–H group of the imidazolium ring, followed by the C<sub>8</sub>–H, C<sub>9</sub>–H groups and methyl group C<sub>19</sub>H<sub>3</sub>. The hydrogen atoms in the methyl group of the imidazolium ring have more positive electrostatic potentials than those in the octyl group. For the [BF<sub>4</sub>]<sup>-</sup> anion, as expected, the region with a negative electrostatic potential, mapped in red, is located around the four fluorine atoms, each of which shares an equal portion of the electrostatic potential.

The most stable configuration for the interaction between the [OMIM]<sup>+</sup> cation and the [BF<sub>4</sub>]<sup>-</sup> anion is presented in Fig. 2c. The interactions between the cation and anion are characterized by multiple interactions formed mainly between the hydrogen atoms of the [OMIM]<sup>+</sup> cation and the fluorine atoms of the [BF<sub>4</sub>]<sup>-</sup> anion. Previous investigations have demonstrated that HBs are the most important and common non-covalent interactions [53–55] play an important role in chemical processes [56–59]. Generally, the sum of the van der Waals radii between the proton on the donor and the acceptor atom is used as the accepted geometric criteria value for judging the formation of HBs [60]. Thus, the HBs will be formed when the distance between the fluorine and hydrogen atoms (F···H) is less than 2.67 Å [61]. HBs are noted by dashed lines, and the corresponding bond lengths are also labeled in Fig. 2c. Moreover, six possible HBs form in the ion pair, and the strongest interaction occurs between F<sub>5</sub> and C<sub>6</sub>–H with a bond length of 2.282 Å. This stable structure will be the basis of our further exploration of the interaction between the ion pair and molecules of solvents.

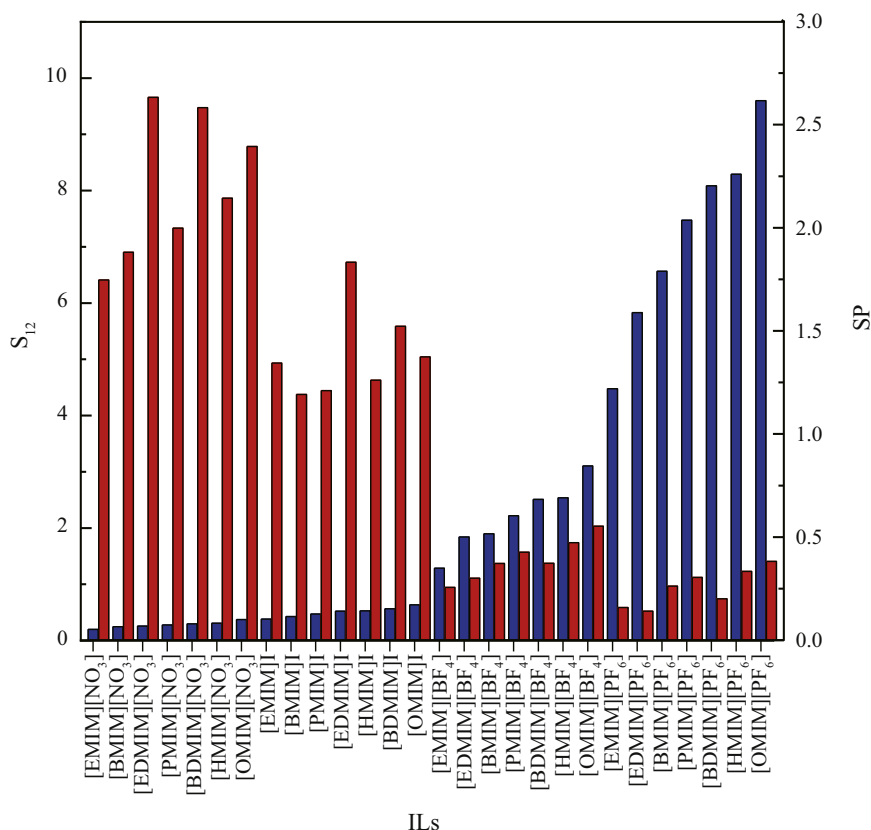


Fig. 1.  $S_{12}$  (blue column) of ethanol to EA in different ILs and SP (red column) calculated by COSMO-RS.

### 3.3. Configuration of ion pair interaction with ethanol/EA

Optimized structures of the ion pair [OMIM][BF<sub>4</sub>], ethanol and EA were screened from 40 initial configurations to find the one with the lowest energy. Again, no imaginary frequencies are found.

Optimized structure of ion pair with ethanol is depicted in Fig. 3a. The ethanol molecule is located at the “top” of the system with two possible HBs formed, including a special hydrogen bond C<sub>6</sub>–H···O<sub>19</sub> and a short interaction is formed between the hydroxyl group and one of the fluorine atoms. The structure formed by [OMIM][BF<sub>4</sub>] and EA in Fig. 3b has three possible HBs. The shortest HB formed in the structure is between the oxygen atom of the carbonyl group and the C<sub>6</sub>–H.

Thermodynamic properties of mixtures are dominated by noncovalent interactions [30,62,63]. To understand the complex interactions formed in the optimized structure, analysis of the noncovalent interactions is required. The nature of interaction within the optimized structures formed between the ion pair [OMIM][BF<sub>4</sub>] and ethanol or EA was characterized by RDG functions. The RDG function was developed by Yang et al. [30] as a simple method for visualizing the noncovalent-interaction area within the whole simulation region. The reduced density gradient  $s$  is developed using following equation:

$$s = \frac{1}{2(3\pi^2)^{\frac{1}{3}}} \cdot \frac{|\nabla\rho|}{\rho^{\frac{4}{3}}} \quad (6)$$

in which  $\rho$  is the quantum-mechanical electron density in this simulation box. This dimensionless quantity  $s$  is typically used to describe the electron density gradient under a homogeneous overall electron distribution. Normalization by  $\rho$  makes sure that even in regions of weak interactions,  $s$  can still properly detect the electron distribution variation. Sign ( $\lambda_2$ ) is the sign of second largest eigenvalue of the electron density Hessian matrix  $\lambda_2$ . By plotting  $s$  versus sign ( $\lambda_2$ ) $\rho$ , the basic pattern of intermolecular interactions could be identified.

RDG isosurface of both structures are visualized in Fig. 4 and plots of RDG versus sign ( $\lambda_2$ ) $\rho$  are shown in Fig. 5. To highlight the main interaction, Fig. 4 only shows regions of sign ( $\lambda_2$ ) $\rho$  ranging from  $-0.04$  to  $-0.02$  au. As shown in Fig. 4a–b, the low density isosurface which is green forms inside the trimer complexes and no prominent dispersion red region is depicted. For comparison with those regions, the blue disks, which represent the main weak interaction regions, are highlighted in red circles. For the two stable configurations, the significant interactions (C<sub>6</sub>–H···O<sub>19</sub>) (O<sub>19</sub>–H···F), and (C<sub>6</sub>–H···O<sub>24</sub>), are captured by the blue isosurfaces. The quantity and size of weak interaction regions in those visualizations reflect the strength of interaction. From the RDG analysis in Fig. 4, we can observe that the stable configuration formed by ILs and ethanol has a larger density isosurface.

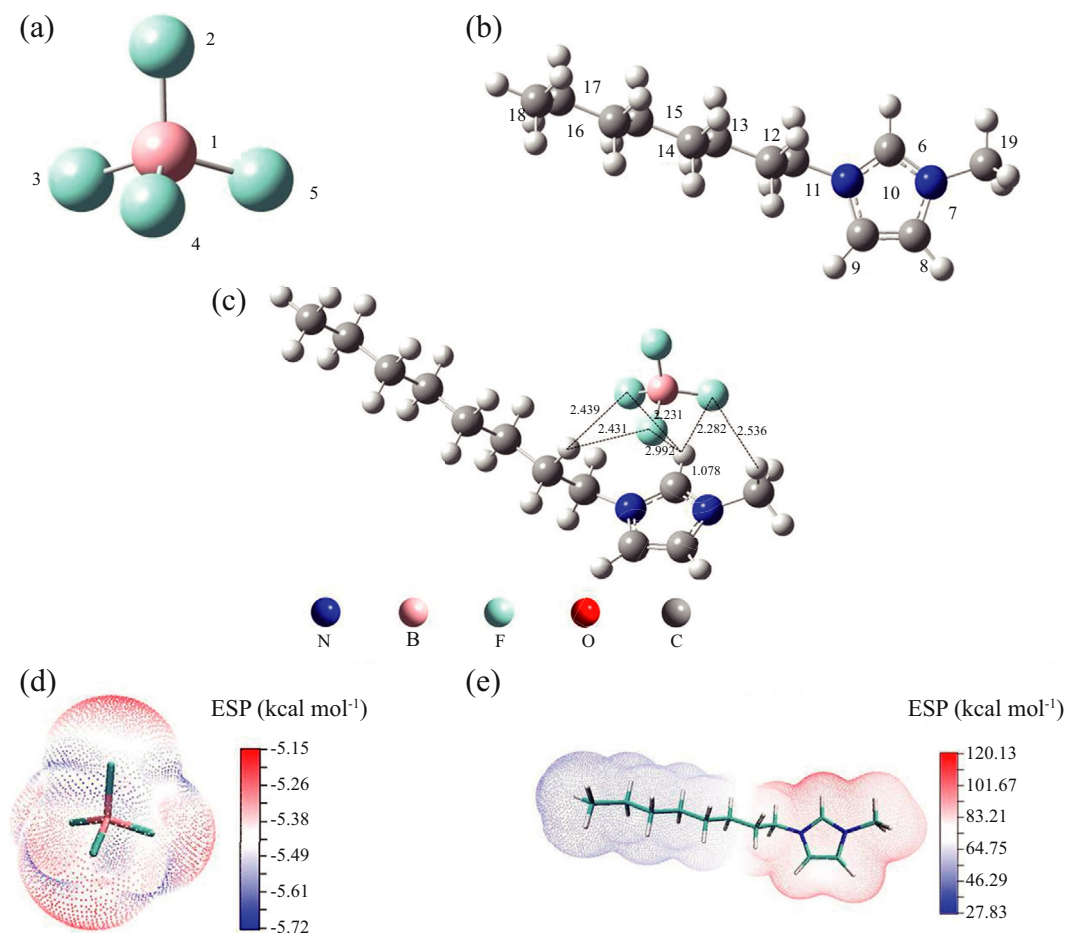


Fig. 2. Optimized geometries of the isolated anion (a)  $[\text{BF}_4]^-$ , (b)  $[\text{OMIM}]^+$ , (c) ion pair and electrostatic potential analysis of (d)  $[\text{BF}_4]^-$  and (e)  $[\text{OMIM}]^+$ .

Fig. 5 also shows more blue spikes within the range of  $-0.04$ – $0.02$  au. in the ethanol- $[\text{OMIM}][\text{BF}_4]$  complex, which indicates the higher contribution of weak interaction.

The results of the QTAIM analysis are provided in Fig. 6. To emphasize the main weak interaction with the structure, the critical points (3, -1) were highlighted and other kinds of critical points were eliminated. The 108th, 109th, 124th bonds corresponds to the main interactions ( $\text{C}_6\text{-H}\cdots\text{O}_{19}$ ) ( $\text{O}_{19}\text{-H}\cdots\text{F}$ ) and ( $\text{C}_6\text{-H}\cdots\text{O}_{24}$ ) which have been discussed above in RDG analysis. The main parameters in QTAIM analysis are shown in Table 1. According to the QTAIM theory, the electron density ( $\rho$ ), Laplacian of electron density ( $\nabla^2\rho$ ), Lagrangian kinetic energy  $G(r)$  Potential energy density  $V(r)$

and total electron density ( $H$ ) quantify a bond's covalency. The Laplacian of  $\rho$ ,  $\nabla^2\rho$  describes the degree of the electron density concentration, which indicates the polarity around the critical point. A positive  $\nabla^2\rho$  indicates a highly polarized bond, while a covalent interaction yields negative  $\nabla^2\rho$ .  $H < 0$  is also considered a sign for covalent bonds [64]. From the result in Table 1, all three main interactions have positive  $\nabla^2\rho$  values and  $H$  values, which clearly indicates a non-covalent character. The strength of interaction mainly depends on the value of electron density  $\rho$ . From the results in Table 1, the two main interaction in the ethanol- $[\text{OMIM}][\text{BF}_4]$  complex has larger  $\rho$  than the ( $\text{C}_6\text{-H}\cdots\text{O}_{24}$ ) interaction in the EA- $[\text{OMIM}][\text{BF}_4]$  complex, which represents a higher interaction

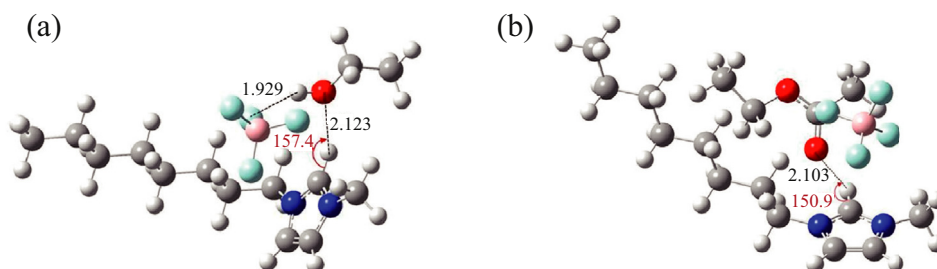


Fig. 3. Optimized geometry of  $[\text{OMIM}][\text{BF}_4]$  ion pairs formed with (a) ethanol and (b) EA.

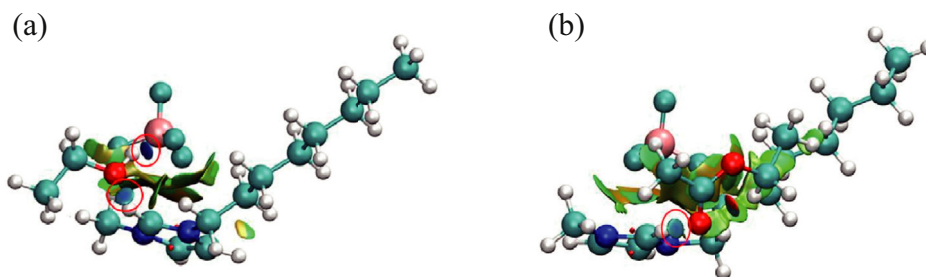


Fig. 4. Reduced density gradient isosurface ( $s = 0.05$ ) for the  $[\text{OMIM}][\text{BF}_4]$  ion pairs with (a) ethanol and (b) EA. The surfaces are colored on a blue-green-red scale according to values of  $\text{sign}(\lambda_2)\rho$ , ranging from  $-0.04$  to  $-0.02$  au.

strength. The result indicates that both main interactions in the ethanol- $[\text{OMIM}][\text{BF}_4]$  complex are stronger than that in the EA- $[\text{OMIM}][\text{BF}_4]$  complex.

Interaction energy is a direct measure of the stability of an optimized structure [65]. By using Eqs. (1) and (2), the BSSE-corrected interaction energies are calculated and shown in Table 2. It is clearly seen that the interaction energy of the ethanol- $[\text{OMIM}][\text{BF}_4]$  complex ( $E_{int}^B = 53.862 \text{ kJ mol}^{-1}$ ) is about  $7 \text{ kJ mol}^{-1}$  higher than that of the ion pair with EA. On the other hand, ethanol dimer, EA dimer and the ethanol-EA pair all have similar interaction energy which is much lower than that of the ion pair with either of solvent molecules. The result reveals that the structures of the ion pair formed with the solvent molecules are more stable than those formed between solvent molecules themselves, which also indicates that  $[\text{OMIM}][\text{BF}_4]$  can break the structure formed by ethanol and EA molecules and reconstruct a more stable one.

### 3.4. Behaviors of $[\text{OMIM}][\text{BF}_4]$ in the azeotropic system

Till now, we have known that in an isolated setting, the interaction between ethanol and  $[\text{OMIM}][\text{BF}_4]$  is stronger than that of complex formed by EA and  $[\text{OMIM}][\text{BF}_4]$ . We now investigate such interactions in the bulk phase where the ion pair is surrounded by a massive amount of solvents and also need to be investigated. Here, we employed molecular dynamics simulation to inspect the solvent effects on the local structure of the ion pair.

At first, to further explore the interaction of ion pair with solvents molecules, the case of a single  $[\text{OMIM}][\text{BF}_4]$

molecule solvated by the ethanol/EA mixture was investigated. As shown in Fig. 7, a geometrically optimized ion pair (using the QM approach above) was placed at the center of the simulation box which is then filled with ethanol and EA molecules. The coordinates of the cation  $[\text{OMIM}]^+$  were fixed during the whole process. During the first half of equilibrium process, the anion  $[\text{BF}_4]^-$  fluctuated quickly and gradually moved from the top of the cation to its downside. After that, it moved back to the initial position, which, again, is accompanied by strong fluctuations. From the whole process, it can be concluded that the structure we obtained from the QM calculation mentioned above is relatively stable even in the solution phase.

To analyze the local structure of the cation, we calculated the spacial distribution function (SDF). SDF is by definition proportional to the possibility of finding a certain type of atoms around a specified reference atom in the 3D space. Fig. 8 shows the calculated three-dimensional structures of SDFs of the hydroxyl  $\text{O}_{19}$  atom in ethanol molecules and those of the carbonyl  $\text{O}_{24}$  atom in EA molecules, both around the cation  $[\text{OMIM}]^+$ . Observation of three large lobes in Fig. 8a, aligning with the  $\text{C}_6\text{-H}$ ,  $\text{C}_8\text{-H}$ ,  $\text{C}_9\text{-H}$  bonds, respectively, indicates that ethanol molecules mainly appear in the vicinity of these three types of bonds. Compared with the isosurface in Fig. 8a, the isosurface formed by carbonyl  $\text{O}_{24}$  in EA molecules is much smaller and more dispersed. This indicates that ethanol molecules have stronger interactions with the cation and gather closer to the imidazole of the cation than the EA molecules.

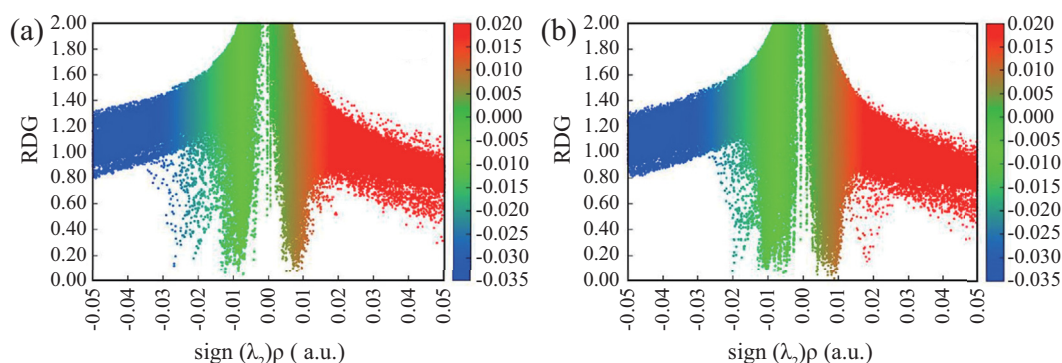


Fig. 5. Plots of the  $\text{sign}(\lambda_2)\rho$  and the reduced electron density gradient  $s$  for (a)  $[\text{OMIM}][\text{BF}_4]$ -ethanol and (b)  $[\text{OMIM}][\text{BF}_4]$ -EA.

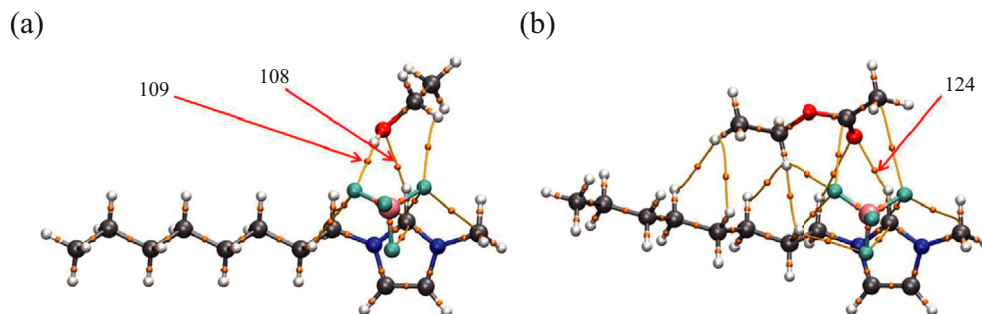


Fig. 6. QTAIM analysis of the optimized structures of (a) [OMIM][BF<sub>4</sub>] with ethanol and (b) [OMIM][BF<sub>4</sub>] with EA.

Table 1  
QTAIM Parameters corresponding to the electron density ( $\rho$ ), Laplacian ( $\nabla^2\rho$ ) and total electron density ( $H$ ).

No.	Bond	$\rho(r)$	$\nabla^2\rho$	$G(r)$	$V(r)$	$H(r)$
108	C <sub>6</sub> –H···O <sub>19</sub>	0.021612	0.081243	0.017716	–0.015120	0.0025953
109	O <sub>19</sub> –H···F	0.027414	0.11933	0.028096	–0.026360	0.0017357
124	C <sub>6</sub> –H···O <sub>24</sub>	0.020092	0.085052	0.017744	–0.014224	0.0035193

The MD simulation was then performed for the cases of different ILs concentrations. As the concentration of the ion pairs increases, the number of H-bonds ( $N_{\text{HB}}$ ) between the solvent molecules was counted and shown in Fig. 7. In our MD simulation, H-bonds are defined using the following

conditions according to the classical geometric criterion [66,67]:

- 1) The distance between the two O atoms of the interacting hydroxyl groups is less than 3.5 Å.
- 2) The bond angle of H–O···O should be less than 30°.

The results in Fig. 9 showed that the number of HB formed between ethanol molecules and that between ethanol and EA both decrease steadily with the increasing mole fraction of the IL. The number of HBs reveals the degree of binding between these two types of solvent molecules and thus its decrease shows that the interaction is weakened between the solvents with increasing IL mole fraction.

Table 2  
The BSSE-corrected interaction energies (kJ mol<sup>–1</sup>) of the ILs-ethanol-EA complexes calculated from Eq. (1).

solvent	With [OMIM][BF <sub>4</sub> ](A)			With ethanol			With EA		
	$E_{\text{int}}$	$E_{\text{BSSE}}$	$E_{\text{int}}^B$	$E_{\text{int}}$	$E_{\text{BSSE}}$	$E_{\text{int}}^B$	$E_{\text{int}}$	$E_{\text{BSSE}}$	$E_{\text{int}}^B$
Ethanol	–58.989	5.127	–53.862	–31.447	3.504	–27.943	–31.636	2.083	–29.553
EA	–53.379	6.700	–46.679				–29.751	4.131	–25.620

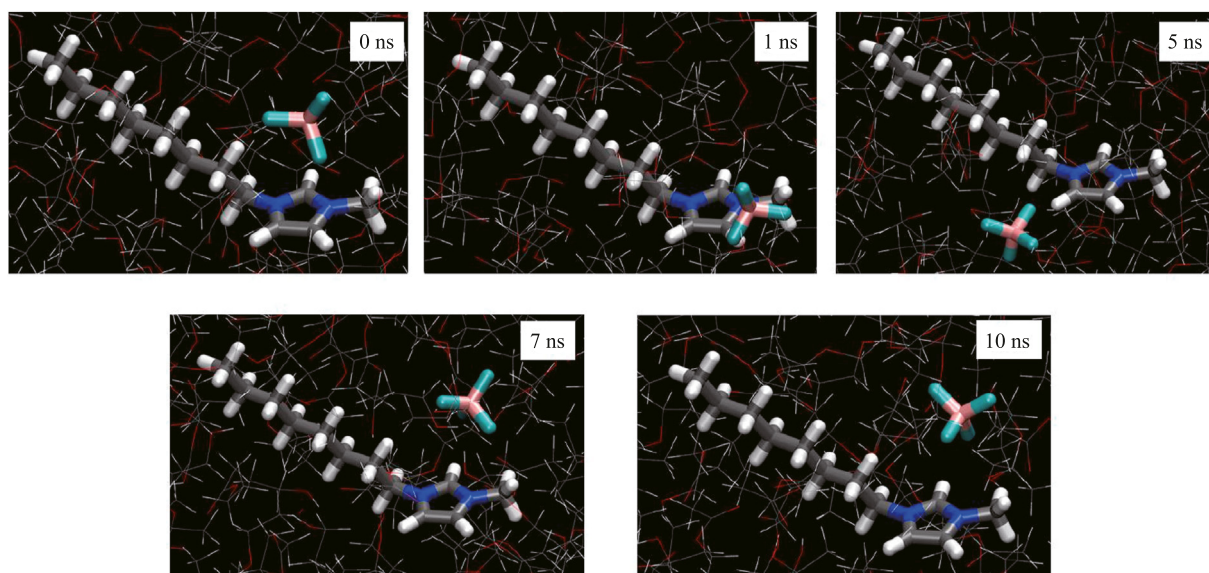


Fig. 7. Configurations of the ion pair [OMIM][BF<sub>4</sub>] at different moments during the simulation.

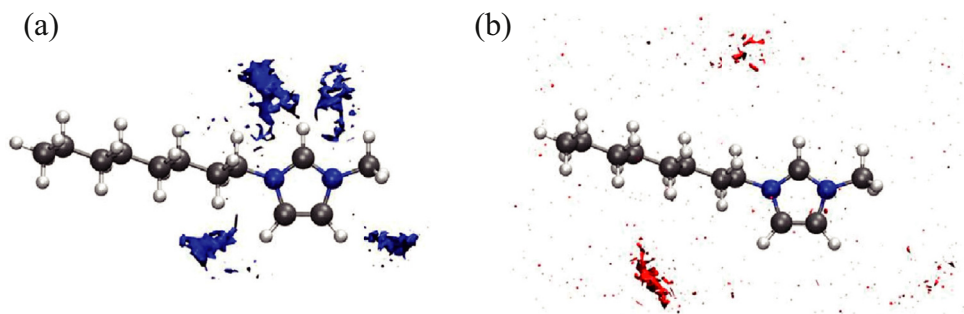


Fig. 8. (a) Colored SDFs (isosurface value:  $0.09 \text{ \AA}^{-3}$ ) of the hydroxyl  $O_{19}$  atom in ethanol molecules around the cation  $[\text{OMIM}]^+$  and (b) Colored SDFs (isosurface value:  $0.06 \text{ \AA}^{-3}$ ) of the carbonyl  $O_{24}$  atom in EA molecules around the cation  $[\text{OMIM}]^+$ .

Radial distribution function (RDF) is also a powerful method to help us get more useful information about the microscopic structure. It reflects the possibility of finding a particle at a certain distance  $r$  away from the chosen molecule. We can also study the relative strength of interactions between two species within the mixture from the RDF.

The RDFs of the cation  $[\text{OMIM}]^+$  with respect to ethanol or EA molecules at different concentrations of the IL were compared in Fig. 10. There are two apparent peaks in the  $[\text{OMIM}]^+$ -ethanol profiles. Both peaks have similar heights. These peaks reflect two solvation shells of ethanol molecules wrapping around the cation and the number densities of ethanol molecules in both shells are quite similar. Compared with the  $[\text{OMIM}]^+$ -ethanol profiles, the  $[\text{OMIM}]^+$ -EA profiles show two much milder peaks at similar positions. This indicates that the  $[\text{OMIM}]^+$  solvation shells around EA molecules appear at similar distances as those around ethanol molecules but have much lower density. Thus, the cation has stronger interaction with ethanol molecules than it does with EA. This is consistent with the previous discussion in this work. Furthermore, the heights of the first peaks in both  $[\text{OMIM}]^+$ -ethanol and  $[\text{OMIM}]^+$ -EA profiles increase as the concentration of ILs increases – i.e., the ability of  $[\text{OMIM}]^+$  binding with solvent molecules increases with the IL mole

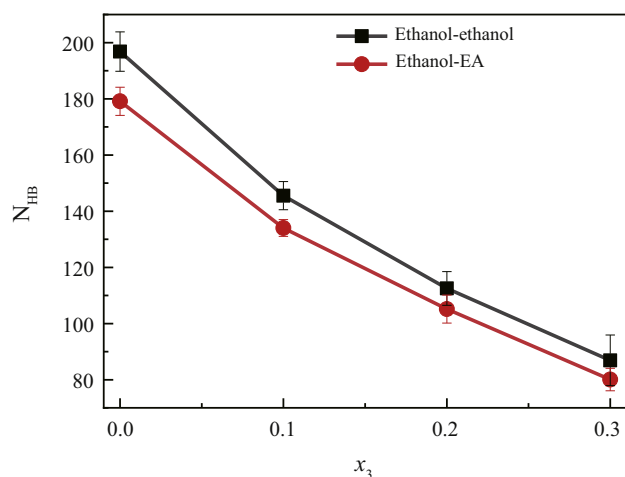


Fig. 9. Number of H-bonds versus the mole fraction of  $[\text{OMIM}][\text{BF}_4]$ .

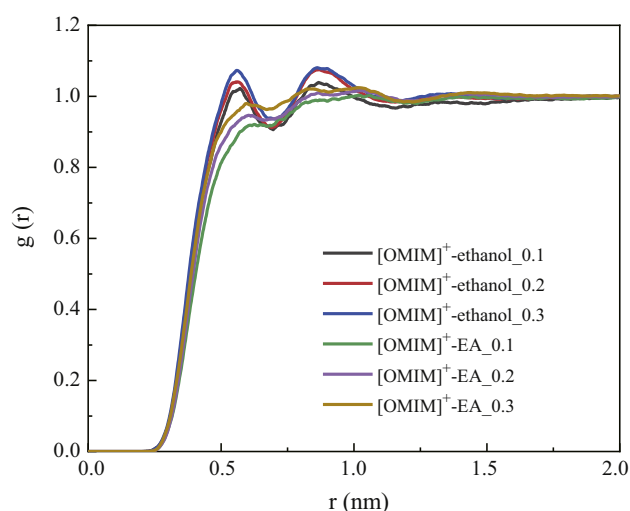


Fig. 10. Radial distribution function versus the distance between  $[\text{OMIM}]^+$  and the center of mass of the ethanol or EA molecules at a mole fraction of ILs ranging from 0.1 to 0.3.

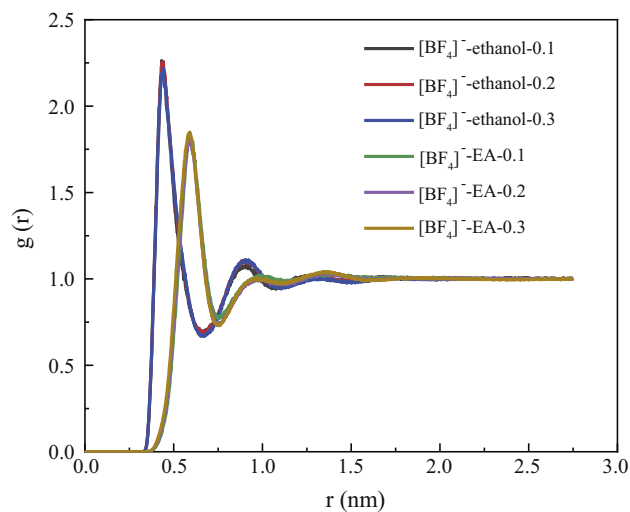


Fig. 11. Radial distribution function versus the distance between the center of  $[\text{BF}_4]^-$  and the center of mass of ethanol or EA molecules with the IL mole fraction ranging from 0.1 to 0.3.

fraction. This again illustrates why the enhanced separation effect becomes more obvious with higher IL loads.

Besides the cation, the RDFs for the anion were also calculated, as shown in Fig. 11. All the peaks for  $[\text{BF}_4]^-$ -ethanol or  $[\text{BF}_4]^-$ -EA are sharper and higher compared with those in Fig. 10. The first peaks for  $[\text{BF}_4]^-$ -ethanol are also higher than those for  $[\text{BF}_4]^-$ -EA. This means the  $[\text{BF}_4]^-$  has a prominent effect of attracting ethanol molecules in this azeotropic system. Compared with the cation, the anion shows closer binding with the solvent molecules, but for different mole fractions of the IL, the shapes and heights of all peaks remain the same, which indicate much weaker concentration effects on the role of  $[\text{BF}_4]^-$  in this separation process.

#### 4. Conclusions

In this paper, the COSMO-RS model was applied to screen an appropriate imidazolium ionic liquid considering the selectivity and solvent capacity. And  $[\text{OMIM}][\text{BF}_4]$  is calculated as a wonderful entrainer. Microstructures and molecular interactions of the ion pair  $[\text{OMIM}][\text{BF}_4]$  and its complexes with  $\text{C}_2\text{H}_5\text{OH}$  and  $\text{CH}_3\text{COOCH}_2\text{CH}_3$  molecules are investigated by DFT calculations and MD simulation. Interactions such as H-bonds and van der Waals forces are explored using the RDG method and QTAIM analysis. The calculation results show that the interaction between EA and ethanol molecules is much weaker than that between the ion pair and either EA or ethanol. Therefore, the initial stable structure formed by ethanol and EA molecules will be broken by the addition of the IL. The results also illustrate that the interaction of the  $[\text{OMIM}][\text{BF}_4]$  ion pair with ethanol is stronger than that of the  $[\text{OMIM}][\text{BF}_4]$  ion pair with EA. The MD simulation reveals that  $[\text{OMIM}][\text{BF}_4]$  has a noticeable effect on reducing the number of HBs between the solvent molecules. The cation is more attracted to the ethanol molecules than it is to EA. Such effect is stronger as the concentration of  $[\text{OMIM}][\text{BF}_4]$  increases. The anion is strongly attracted to both solvent species, but such effect is insensitive to the IL concentration. This study contributes to the deeper understanding into the mechanism of interaction between azeotropes and entrainers, which facilitates the selection and design of suitable IL extractants for extractive distillation processes.

#### Conflict of interest

The authors declare that they have no known competing financial interests or personal relationships that could have appeared to influence the work reported in this paper.

#### Acknowledgments

The authors are grateful to the financial support from the Program for the National Key R&D Program of China (2018YFB0604900) and the National Natural Science Foundation of China (No. 21878219). L.X. acknowledges the financial support by the Natural Sciences and Engineering Research Council (NSERC) of Canada (RGPIN-4903-2014).

D. L. acknowledges China Scholarship Council (CSC) for supporting his doctoral study at McMaster University (No. 201500090106).

#### References

- [1] Z. Lei, C. Dai, J. Zhu, B. Chen, *AIChE J.* 60 (2014) 3312–3329.
- [2] Z. Lei, B. Chen, Z. Ding, *Special Distillation Processes*, Elsevier Science, Amsterdam, 2005.
- [3] V. Dohnal, E. Baránková, A. Blahut, *Chem. Eng. J.* 237 (2014) 199–208.
- [4] J.F. Wang, J.Q. Luo, S.C. Feng, H.R. Li, Y.H. Wan, X.P. Zhang, *Green Energy Environ.* 1 (2016) 43–61.
- [5] H.H. Zhang, M.Y. Zhu, W. Zhao, S. Li, G. Feng, *Green Energy Environ.* 3 (2018) 120–128.
- [6] M.L. Mu, J. Cheng, C.N. Dai, N. Liu, Z.G. Lei, Y.Z. Ding, J.J. Lu, *Green Energy Environ.* 4 (2019) 190–197.
- [7] Q. Li, W. Zhu, Y. Fu, H. Wang, L. Li, B. Wang, *J. Chem. Eng. Data* 57 (2012) 1602–1606.
- [8] X. Chen, F. Cai, X. Wu, C. Asumana, G. Yu, *J. Chem. Eng. Data* 58 (2013) 1186–1192.
- [9] H. Li, J. Zhang, D.Y. Li, X.G. Li, X. Gao, *Mol. Simulat.* 43 (2017) 1125–1133.
- [10] E. Boli, E. Voutsas, *Chem. Eng. Sci.* 219 (2020) 115579.
- [11] A.V. Orchilles, P.J. Miguel, E. Vercher, A. Martinez-Andreu, *J. Chem. Eng. Data* 52 (2007) 141–147.
- [12] Z. Song, X. Hu, Y. Zhou, T. Zhou, Z. Qi, K. Sundmacher, *AIChE J.* 65 (2019) e16625.
- [13] W.X. Zhang, X.B. Liu, H.R. Zhang, S.H. Li, J.W. Yang, P.Z. Cui, Z.Y. Zhu, Y.X. Ma, Y.L. Wang, *ACS Sustain. Chem. Eng.* 7 (2019) 18093–18104.
- [14] Y.J. Hu, F.H. Li, S.N. Wei, S.M. Jin, W.F. Shen, *Separ. Purif. Technol.* 242 (2020) 116829.
- [15] Y. Xu, D.P. Meng, H.Y. Li, X.P. Yu, Z.Y. Zhu, Y.L. Wang, Y.X. Ma, J. Gao, *ACS Sustain. Chem. Eng.* 7 (2019) 19984–19992.
- [16] P. Brault, W. Chamorro-Coral, S. Chuon, A. Caillard, J.M. Bauchire, S. Baranton, C. Coutanceau, E. Neyts, *Front. Chem. Sci. Eng.* 13 (2019) 324–329.
- [17] H. Xu, Z. Han, D.J. Zhang, J.H. Zhan, *ACS Appl. Mater. Interfaces* 4 (2012) 6646–6653.
- [18] W.X. Zhang, Z.R. Chen, Y.Y. Shen, G.X. Li, Y. Dai, J.G. Qi, Y.X. Ma, S. Yang, Y.L. Wang, *ACS Sustain. Chem. Eng.* 8 (2020) 8700–8712.
- [19] F. Chen, L. Zhang, Z. Liu, G. Yu, *Ind. Eng. Chem. Res.* 59 (2020) 13271–13282.
- [20] Q.S. Li, J.G. Zhang, Z.G. Lei, J.Q. Zhu, J.J. Zhu, X.Q. Huang, *Ind. Eng. Chem. Res.* 48 (2009) 9006–9012.
- [21] A. Klamt, F. Eckert, *Fluid Phase Equil.* 172 (2000) 43–72.
- [22] J.L. Han, C.N. Dai, G.Q. Yu, Z.G. Lei, *Green Energy Environ.* 3 (2018) 247–265.
- [23] A. Klamt, F. Eckert, M. Diedenhofen, *Fluid Phase Equil.* 285 (2009) 15–18.
- [24] K. Nakajoh, M. Grabda, S. Oleszek-Kudlak, E. Shibata, F. Eckert, T. Nakamura, *J. Mol. Struct-Theochem* 895 (2009) 9–17.
- [25] A. Navas, J. Ortega, R. Vreekamp, E. Marrero, J. Palomar, *Ind. Eng. Chem. Res.* 48 (2009) 2678–2690.
- [26] A. Klamt, V. Jonas, T. Burger, J.C.W. Lohrenz, *J. Phys. Chem.* 102 (1998) 5074–5085.
- [27] Y. Zhao, D.G. Truhlar, *Theor. Chem. Acc.* 120 (2008) 215–241.
- [28] M.J. Frisch, G.W. Trucks, H.B. Schlegel, G.E. Scuseria, M.A. Robb, J.R. Cheeseman, G. Scalmani, V. Barone, G.A. Petersson, H. Nakatsuji, X. Li, M. Caricato, A. Marenich, J. Bloino, B.G. Janesko, R. Gomperts, B. Mennucci, H.P. Hratchian, J.V. Ortiz, A.F. Izmaylov, J.L. Sonnenberg, D. Williams-Young, F. Ding, F. Lipparini, F. Egidi, J. Goings, B. Peng, A. Petrone, T. Henderson, D. Ranasinghe, V.G. Zakrzewski, J. Gao, N. Rega, G. Zheng, W. Liang, M. Hada, M. Ehara, K. Toyota, R. Fukuda, J. Hasegawa, M. Ishida, T. Nakajima, Y. Honda, O. Kitao, H. Nakai, T. Vreven, K. Throssell, J.A. Montgomery Jr., J.E. Peralta, F. Ogliaro, M. Bearpark, J.J. Heyd, E. Brothers, K.N. Kudin, V.N. Staroverov,

- T. Keith, R. Kobayashi, J. Normand, K. Raghavachari, A. Rendell, J.C. Burant, S.S. Iyengar, J. Tomasi, M. Cossi, J.M. Millam, M. Klene, C. Adamo, R. Cammi, J.W. Ochterski, R.L. Martin, K. Morokuma, O. Farkas, J.B. Foresman, D.J. Fox, Gaussian 09, Revision A.02, Gaussian, Inc., Wallingford CT, 2009.
- [29] S.F. Boys, F.D. Bernardi, *Mol. Phys.* 19 (1970) 553–566.
- [30] E.R. Johnson, S. Keinan, P. Mori-Sánchez, J. Contreras-García, A.J. Cohen, W. Yang, *J. Am. Chem. Soc.* 132 (2010) 6498–6506.
- [31] R.F.W. Bader, *Chem. Rev.* 91 (1991) 893–928.
- [32] T. Lu, F. Chen, *J. Comput. Chem.* 33 (2012) 580–592.
- [33] W. Humphrey, A. Dalke, K. Schulten, *J. Mol. Graph.* 14 (1996) 33–38.
- [34] M.J. Abraham, T. Murtola, R. Schulz, S. Páll, J.C. Smith, B. Hess, E. Lindahl, *SoftwareX* 1–2 (2015) 19–25.
- [35] B. Hess, C. Kutzner, D. van der Spoel, E. Lindahl, *J. Chem. Theor. Comput.* 4 (2008) 435–447.
- [36] W.L. Jorgensen, D.S. Maxwell, J. Tirado-Rives, *J. Am. Chem. Soc.* 118 (1996) 11225–11236.
- [37] X. Li, J. Liu, K. Lin, Y. Zhang, Y. Zhang, R. Zheng, Q. Shi, Y. Guo, Z. Lu, *J. Phys. Chem. C* 123 (2019) 12975–12983.
- [38] J. Liu, X. Li, J. Hou, X. Li, Z. Lu, *Langmuir* 35 (2019) 7050–7059.
- [39] J.G. McDaniel, E. Choi, C.Y. Son, J.R. Schmidt, A. Yethiraj, *J. Phys. Chem. B* 120 (2016) 231–243.
- [40] K. Goloviznina, J.N.C. Lopes, M.C. Gomes, A.A.H. Padua, *J. Chem. Theor. Comput.* 15 (2019) 5858–5871.
- [41] B. Doherty, O. Acevedo, *Abstr. Pap. Am. Chem. Soc.* 257 (2019) 1.
- [42] L.S. Dodda, I.C. de Vaca, J. Tirado-Rives, W.L. Jorgensen, *Nucleic Acids Res.* 45 (2017) W331–W336.
- [43] W.L. Jorgensen, J. Tirado-Rives, *Proc. Natl. Acad. Sci. U. S. A* 102 (2005) 6665–6670.
- [44] L.S. Dodda, J.Z. Vilseck, J. Tirado-Rives, W.L. Jorgensen, *J. Phys. Chem. B* 121 (2017) 3864–3870.
- [45] S.V. Sambasivarao, O. Acevedo, *J. Chem. Theor. Comput.* 5 (2009) 1038–1050.
- [46] B. Doherty, X. Zhong, S. Gathiaka, B. Li, O. Acevedo, *J. Chem. Theor. Comput.* 13 (2017) 6131–6145.
- [47] L. Martinez, R. Andrade, E.G. Birgin, J.M. Martinez, *J. Comput. Chem.* 30 (2009) 2157–2164.
- [48] G. Bussi, D. Donadio, M. Parrinello, *J. Chem. Phys.* 126 (2007) 014101.
- [49] U. Essmann, L. Perera, M.L. Berkowitz, T. Darden, H. Lee, L.G. Pedersen, *J. Chem. Phys.* 103 (1995) 8577–8593.
- [50] J. Zhu, H. Qi, B. Sun, H. Fan, X. Zhang, *J. Mol. Liq.* 319 (2020) 114159.
- [51] L. Cao, P.P. Liu, B.H. Wang, Q.S. Li, *Fluid Phase Equil.* 372 (2014) 49–55.
- [52] Z.Y. Zhu, X.L. Geng, W. He, C. Chen, Y.L. Wang, J. Gao, *Ind. Eng. Chem. Res.* 57 (2018) 9656–9664.
- [53] K. Matsumoto, R. Hagiwara, *J. Fluor. Chem.* 128 (2007) 317–331.
- [54] A.R. Choudhury, N. Winterton, A. Steiner, A.I. Cooper, K.A. Johnson, *J. Am. Chem. Soc.* 127 (2005) 16792–16793.
- [55] J.D. Holbrey, W.M. Reichert, R.D. Rogers, *Dalton Trans.* (2004) 2267–2271.
- [56] A. Aggarwal, N.L. Lancaster, A.R. Sethi, T. Welton, *Green Chem.* 4 (2002) 517–520.
- [57] W.D. Arnold, E. Oldfield, *J. Am. Chem. Soc.* 122 (2000) 12835–12841.
- [58] H. Sun, S.J. Mumby, J.R. Maple, A.T. Hagler, *J. Am. Chem. Soc.* 116 (1994) 2978–2987.
- [59] G.A. Jeffrey, G.A. Jeffrey, *An Introduction to Hydrogen Bonding*, Oxford University Press, New York, 1997.
- [60] H. He, S. Zhang, X. Liu, J. Wang, X. Yao, X. Zhang, *Fluid Phase Equil.* 360 (2013) 169–179.
- [61] K.H. Liu, M. Pu, H.Y. Li, B.H. Chen, *Chin. J. Chem. Phys.* 18 (2005) 331–335.
- [62] S.S. Sheiko, F.C. Sun, A. Randall, D. Shirvanyants, M. Rubinstein, H. Lee, K. Matyjaszewski, *Nature* 440 (2006) 191–194.
- [63] H. Fenniri, M. Packiarajan, K.L. Vidale, D.M. Sherman, K. Hallenga, K.V. Wood, J.G. Stowell, *J. Am. Chem. Soc.* 123 (2001) 3854–3855.
- [64] V.E.J. Berryman, J.J. Shephard, T. Ochiai, A.N. Price, P.L. Arnold, S. Parsons, N. Kaltsoyannis, *Phys. Chem. Chem. Phys.* 22 (2020) 16804–16812.
- [65] H. Li, P. Zhou, J. Zhang, D.Y. Li, X.G. Li, X. Gao, *J. Mol. Liq.* 251 (2018) 51–60.
- [66] P. Sillren, J. Bielecki, J. Mattsson, L. Borjesson, A. Matic, *J. Chem. Phys.* 136 (2012) 094514.
- [67] D.Y. Li, Z.Q. Gao, N.K. Vasudevan, H. Li, X. Gao, X.G. Li, L. Xi, *J. Phys. Chem. B* 124 (2020) 3371–3386.